NbReN: A disordered superconductor in thin film form for potential application as superconducting nanowire single photon detector

C. Cirillo,[1] V. Granata,[2] A. Spuri,[3] A. Di Bernardo,[3] and C. Attanasio[2]
[1]*CNR-SPIN, c/o Università degli Studi di Salerno, I-84084 Fisciano (Sa), Italy*
[2]*Dipartimento di Fisica "E.R. Caianiello", Università degli Studi di Salerno, I-84084 Fisciano (Sa), Italy*
[3]*Universität Konstanz, Fachbereich Physik, Universitätsstraße 10, 78457 Konstanz, Germany*

(Received 18 December 2020; accepted 16 July 2021; published 9 August 2021)

A superconductor, NbReN, in thin film form is synthesized. Here, the deposition parameters and the electrical transport characterization of NbReN films grown by reactive dc sputtering using a NbRe target are reported. The deposition conditions are systematically varied to optimize the superconducting and electrical properties of the resulting samples. Films with polycrystalline structure and well established superconducting ordering are obtained. The results of the electrical transport properties are studied and interpreted in the framework of different theoretical models. From the analysis of the estimated microscopical parameters considerations about research perspectives as well as possible future applications of the material are discussed. In particular, the potential of NbReN thin films for the realization of SNSPDs with improved performances compared to the existing ones is evaluated.

DOI: 10.1103/PhysRevMaterials.5.085004

I. INTRODUCTION

The continuously increasing demand for superconducting nanowire single photon detectors (SNSPDs) with improved performances compared to existing ones fosters the research activity in the field of material science [1–3]. The current challenge is twofold and consists, on one hand, of improving the properties of superconducting materials already established for the fabrication of SNSPDs (mostly transition metal nitrides, such as NbN and NbTiN) [4–9], and, on the other hand, of finding alternative materials that can improve specific figures of merit of the existing SNSPD devices. Amorphous superconductors (WSi, MoGe, MoSi, NbSi) [10–14] can help to achieve the latter objective, since they combine high potential for applications in the field of quantum technology [1,15] with fabrication advantages, such as high homogeneity, easy pattering, and free substrate choice. A vast class of materials, such as MgB_2 [16], MoN [17], Nb-C [18], cuprate superconductors [19], as well as $NbSe_2$ flakes [20], were also tested. In this constant research for novel superconducting materials which could help to overcome the limits of current devices, the proposal for testing the performance of NbRe [21], a noncentrosymmetric superconductor, was recently put forward [22]. The analysis of the microscopic parameters which characterize the material (e.g., short quasiparticle relaxation rates, small crystallites, large expected hot-spot radius) and the comparison of these figures with the ones of common crystalline materials of choice in this field as well as of amorphous superconductors, along with the intermediate value of the superconducting energy gap, indicate thet NbRe is a promising candidate for the realization of fast SNSPDs [22]. Indeed, the performances of the first NbRe-based SNSPDs are encouraging, featuring a saturated internal efficiency up to $\lambda \approx 1.3$ μm, recovery times between about 8 and 19 ns, and a jitter of about 35 ps at about $T = 3$ K [23]. As a result, this work opens a route to future experiments for improving the performance of these detectors. In particular, along with the tuning of the microscopical parameters of the material suggested in Ref. [23], here the synthesis of nitrated NbRe films is pursued. Compared to NbRe, the nitrated NbRe films are expected to have an enhanced sheet resistance [24] which should produce larger hot spots (HS), shorter rise time, and better optical absorption [1]. Historically, the interest in superconducting nitrides was related to the achievement of higher superconducting critical temperature T_c [25], whereas, more generally, transition metal nitrides are good candidates for different kinds of applications because of their peculiar mechanical and electric properties [24,26]. In the case of NbRe nitride, due to the complex and large unit cell of NbRe [27], it is not straightforward to make predictions about its crystal structure and inversion symmetry, but in principle a noncentrosymmetric crystal structure and a consequently time reversal symmetry breaking with singlet-triplet mixing cannot be excluded [28]. However, it is reasonable to expect that lattice disorder may play a role, with detrimental effects on T_c. The possible presence of mixed phase compositions, widely reported for other nitrides as NbN [29], NbTiN [6], or MoN [17], may complicate the fabrication process. On the other hand, amorphous films with moderate critical temperature in the field of SNSPD may imply less strict growth and patterning requirements and good sensitivity at longer wavelength [1], respectively. In this work superconducting NbRe nitride (hereafter NbReN) films were reactively deposited by carefully tuning the sputtering conditions in a UHV system. The electrical transport properties of the films were investigated to determine the fundamental characteristics of the material.

TABLE I. Deposition conditions and thicknesses of the four main samples series under study.

Series name	P_{tot} (μbar)	$N_2^{\%}$	W (W)	d_{NbReN} (nm)
13S	13	23–38.5	100	36
8S	8	29–37.5	100	36
4.5S	4.5	24–44	150	36
4.5S31-d	4.5	31	150	4–70

The resulting data were analyzed in the framework of different models to shed a light onto the transport mechanisms in the material which are deeply linked to its microscopical structure. This information is essential to clarify the fundamental properties of the material, as well as its possible future applications in the field of SNSPDs. In the conclusions the perspectives of this work are delineated.

II. EXPERIMENT

NbReN films were reactively sputtered in a UHV dc magnetron system starting from a stoichiometric NbRe ($Nb_{0.15}Re_{0.85}$) target of 5 cm in diameter. The system base pressure was in the high 10^{-9} mbar range and the sputtering pressure, monitored by a capacitive gauge, was finely tuned by controlling the amount of argon (Ar) inert gas and nitrogen (N_2) reactive gas flowing via two micrometrical needle valves. Since the quality of superconducting nitride films strongly depends on the proper nitridation of the starting target material [30,31], the deposition at the desired N_2 percentage was realized after saturating the target.

Several sputtering runs were performed in order to find the optimal deposition conditions. The influence of the total gas pressure (P_{tot}), the relative amount of N_2 in the gas mixture [$N_2^{\%} = N_2/(N_2+Ar)$], and the sputtering power (W) on the T_c of the resulting thin films was studied [29–32]. The different substrates explored so far seem to not substantially affect the samples' quality, therefore the paper mainly focuses on films deposited on Si(100) substrates at room temperature. The sputtering rate, measured by a quartz crystal monitor calibrated by a Bruker DektakXT profiler and x-ray reflectometry (XRR) measurements on dedicated films, is in the range 0.03–0.12 nm/s, and it strongly depends on both P_{tot} and W. Different samples' series were deposited. Three sets with a constant thickness of $d_{NbReN} = 36$ nm were realized by fixing both P_{tot} and W and varying $N_2^{\%}$ to study the effect of this parameter on the T_c. The thickness dependence of the superconducting critical temperature with fixed values of P_{tot}, W, and $N_2^{\%}$ was also studied in an additional sample set dedicated to this purpose.

These series of samples, their names and thicknesses, as well as the corresponding deposition conditions, are summarized in Table I. For the sake of clarity, each sample of the three series at constant thickness ($d_{NbReN} = 36$ nm) was named as S forerun by a number indicating the total gas sputtering pressure in μbar and followed by another number which stands for the N_2 percentage used for the deposition. For example, 4.5S27 is the NbReN film 36-nm thick, deposited at $P_{tot} = 4.5$ μbar and $N_2^{\%} = 27$. The series

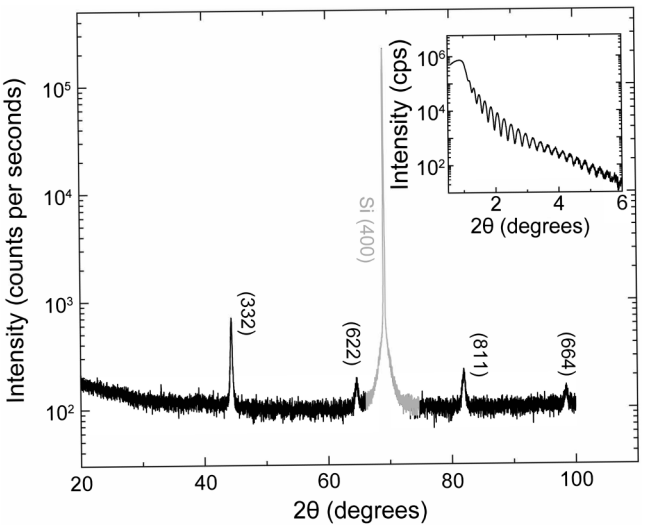

FIG. 1. High-angle x-ray diffraction data for a 36-nm-thick NbReN thin film grown on a Si substrate. The Si(400) substrate diffraction peak is highlighted in gray. The inset shows the low-angle x-ray reflectometry performed on the same NbReN thin film with Kiessig fringes visible up to 6 degrees.

4.5S31-d refers to the set of samples with variable d_{NbReN}. The nomenclature is the same as above, apart from the last suffix which gives the film thickness in nm. The electrical transport measurements were performed in a liquid ^{4}He cryostat by using a custom-made dip probe by using a standard four-wire configuration. The Van der Pauw method [33] was used to determine the resistivity of the unpatterned samples. The structural characterization of the NbReN thin films was performed using x-ray diffractometry (XRD). XRD measurements were carried out using a Rigaku Smartlab diffractometer whose primary arm is equipped with a double-bounce channel cut Ge(220) monochromator to obtain a monochromatic CuKα1 ($\lambda = 1.5406$ Å) radiation.

III. RESULTS

A. X-ray characterization

High-angle $2\theta - \omega$ scan measured on a NbReN thin film (Fig. 1) shows that the NbReN thin films grown on (100)-oriented Si substrates and investigated in this study are polycrystalline. The diffraction planes corresponding to the peaks in Fig. 1 are labeled using the x-ray powder diffraction data available in the literature for NbRe [34,35], under the assumption that the unit cell of NbReN does not significantly differ from that of the parent compound NbRe. Based on the full width at half maximum of the measured x-ray diffraction peaks, using the Scherrer's formula with Patterson correction [36] we estimate a size of the crystallites between 15 and 30 nm, depending on their orientation. Low-angle x-ray reflectometry measurements performed on the same NbReN thin film are shown in the inset of Fig. 1. From the analysis of the XRR scan, it results that the NbReN thin film has a thickness $d_{NbReN} = 35 \pm 0.5$ nm and density $\delta = 13.15 \pm 0.1$ g/cm^3, and it is covered by a top oxide passivation layer with thickness of 1.8 ± 0.1 nm and density 9.23 ± 0.2 g/cm^3.

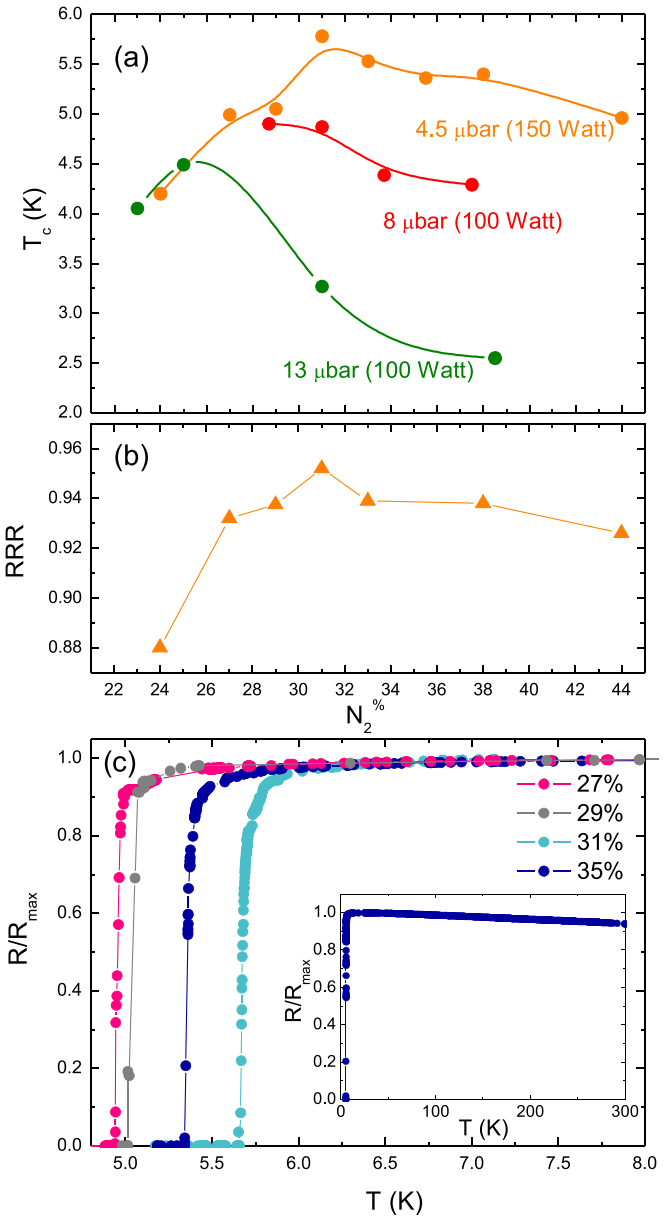

FIG. 2. (a) Critical temperature, T_c, as a function of $N_2^{\%}$ for the three samples' series with $d_{NbReN} = 36$ nm and deposited at different sputtering conditions (see labels). (b) RRR as a function of $N_2^{\%}$ for the films of the series 4.5S. (c) Normalized resistive transition, R/R_{max}, for a selection of samples of the series 4.5S. Inset: The transition of the film 4.5S36 is reported in the full temperature range to give evidence of the increase of the resistance when lowering T.

B. Superconducting critical temperatures

It is well accepted that all the deposition parameters may contribute in a different way and to a different extent to the electrical, structural, and compositional properties of the thin films [37]. The dramatic influence of the sputtering conditions on the critical temperature of NbReN films is synthesized in Fig. 2(a), where T_c (defined at the 90% of the normal state resistivity, R_{max}, evaluated at $T = 20$ K) as a function of the nitrogen percentage is plotted for different values of the total sputtering pressure. It emerges that by decreasing P_{tot}, which also produces an increase in the sputtering rates, the critical temperature generally increases. The curves at fixed total pressure present a maximum, which shifts to higher N_2 concentration as P_{tot} is reduced, in accordance with what is reported for NbN [29,32]. The maximum T_c lies in the range between 4.49 K, obtained for $P_{tot} = 13$ μbar $N_2^{\%} = 25$, and 5.78 K, reached for $P_{tot} = 4.5$ μbar and $N_2^{\%} = 31$ (here also an increase of the sputtering power was applied). Unfortunately, the control of the gas flow in the sputtering system was not enough accurate to set the total pressure below the limit of $P_{tot} = 4.5$ μbar. It is worth noticing that normal state and superconducting properties well correlate each other. This can be inferred from the dependence of the residual resistivity ratio RRR as a function of $N_2^{\%}$, reported in Fig. 2(b) for the series 4.5S. The residual resistivity ratio, defined as the ratio of the resistivity at room temperature and at 20 K, $RRR = \rho_{300}/\rho_{20}$, nicely mimics the $T_c(N_2^{\%})$ behavior with a maximum at $N_2^{\%} = 31$, which indicates that the films having larger critical temperature are more metallic. This result reflects the fact that the optimization of the sputtering conditions leads to less disordered films [29,32]. For both NbReN and NbRe the values of the residual resistivity ratio for the samples with larger T_c is of the order of $RRR \approx 0.95$.

A representative set of the $R(T)$ curves measured for samples grown at different nitrogen flow rates (belonging to the 4.5S series) is shown in Fig. 2(c). In the inset the $R(T)$ curve over the complete temperature range is shown for the sample 4.5S36. As for all the other investigated thin films, the $R(T)$ curve in the inset of Fig. 2(c) also has a residual resistivity ratio less than unity, which is typical of the conduction of dirty metals [32,38]. In this figure, data for lower nitrogen flow were not reported since they correspond to not nitrated films. The chemical composition of the films was in fact systematically measured by energy dispersive spectroscopy on all the samples shown in Fig. 2. This analysis indicates that the optimal film composition, leading to the maximum T_c, corresponds to the atomic concentration ratio $N_2/NbRe = 1.0 \pm 0.2$.

In order to investigate the dependence of the superconducting properties on d_{NbReN}, films of different thickness were also realized. This study is mandatory for a possible application of NbReN in the field of SNSPD, where ultrathin films, with d_{NbReN} comparable to the value of the superconducting coherence length, are needed. The growth recipe of the 45S31 sample was followed and in this way the series named 4.5S31-d was deposited. The normalized resistive transitions for a selection of films belonging to this series are shown in Fig. 3(a). The most promising result is that even the thinnest deposited film, with $d_{NbReN} = 4$ nm, presents a smooth $R(T)$ with a $T_c = 2.72$ K, RRR = 0.77, and $\rho_{20} = 167$ $\mu\Omega$ cm. In Fig. 3(b) is reported the behavior of $T_c(d_{NbReN})$, which shows the typical decrease of the critical temperature as d_{NbReN} is reduced. The highest transition temperature for the film 70-nm thick is $T_c = 5.52$ K, with RRR = 0.94 and $\rho_{20} \approx 177$ $\mu\Omega$ cm. Concerning the estimated resistivity values, it is worth it to comment that they are larger than the ones measured for NbRe [21], a result which is extremely important in view of possible application of NbReN in the field of photon detection. Figure 3(b) displays also the width of the resistive transitions, defined as $\Delta T_c = T_c^{90\%} - T_c^{10\%}$ (right scale, red open

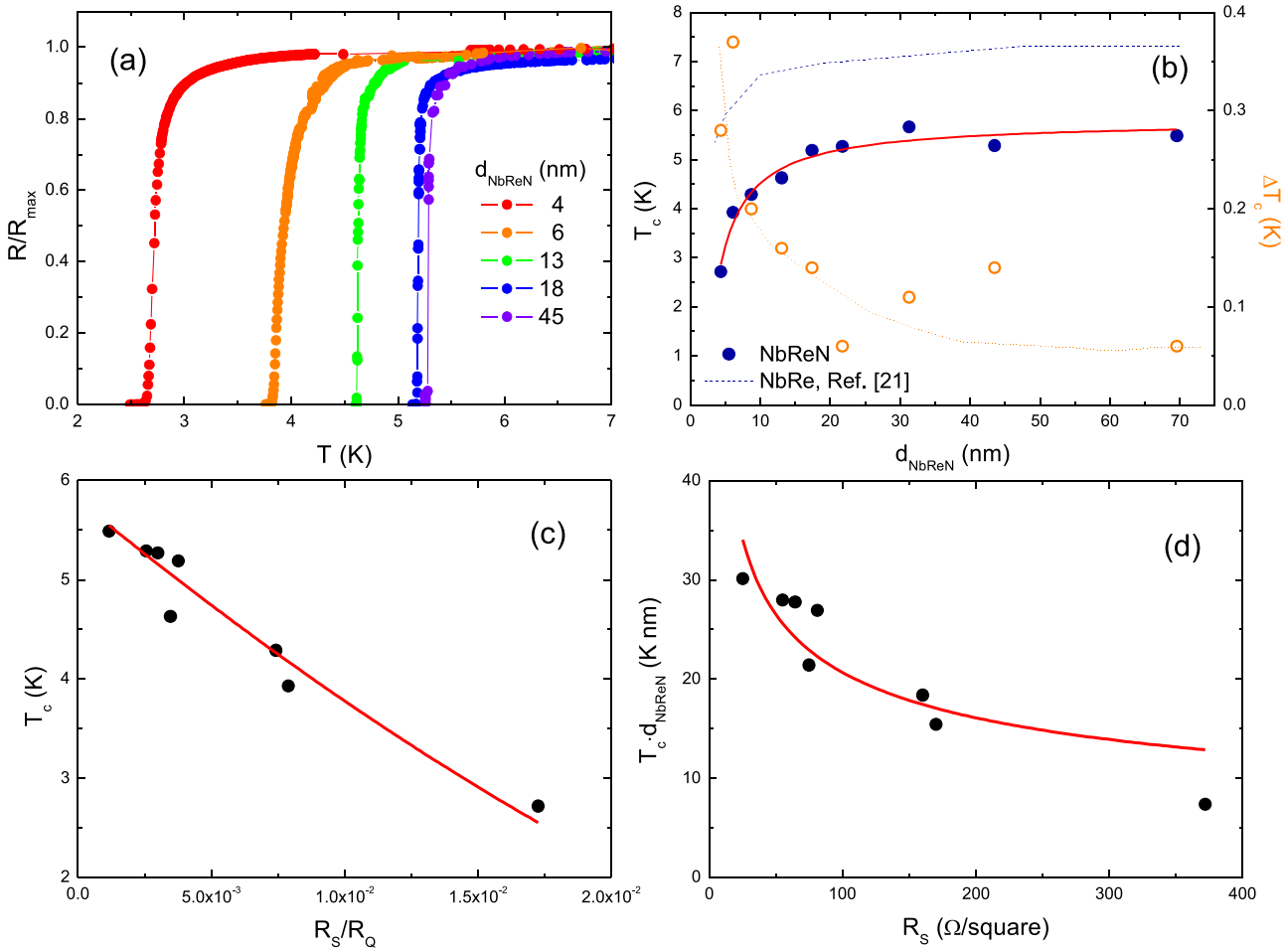

FIG. 3. (a) Normalized resistive transition, $R/R_{\max}$, for a selection of samples of the series at variable thickness, 4.5S31-d. (b) (Left scale) The thickness dependence of the superconducting critical temperature T_c is displayed as blue filled circles. The thick red line is the fit to the $T_c(d)$ data according to the model of Ref. [43]. The same dependence obtained for NbRe is reported as a blue dotted line for comparison. (Right scale) The superconducting transition width ΔT_c as a function of the film thickness is displayed as orange open symbols. The red dotted line is a guide to the eye. (c) Critical temperature as a function of the ratio R_S/R_Q. The red line is the fit according to the Finkel'stein model [44]. (d) Dependence of the product $T_c \cdot d$ on the sheet resistance together with the fit according to the universal scaling law proposed in Ref. [47]. All the data points refer to the films of the series 4.5S31-d.

symbols), which never exceeds 0.4 K. The $T_c(d_{\mathrm{NbReN}})$ data are also compared to the same dependence of NbRe films [21], displayed as a thin blue line. From this comparison it emerges that at the saturation T_c^{NbRe} exceeds the critical temperature of the thick NbReN films of almost 2 K, a result which indicates that further optimization of the deposition conditions should be developed. In this respect, with more information about the crystal structure of the material resulting from the nitrogen incorporation it may be possible to perform energy calculations which could give indications about the expected electronic properties of the system, including T_c [39,40]. The information about the atom positions in the unit cell could be obtained from neutron scattering experiments. Anyway, efforts should be made to obtain highly textured films. However, this task may not be straightforward since the crystal structure of NbRe itself is already quite complex, with a unit cell of 58 atoms, and that the system is generally nonstoichiometric with intrinsic site disorder [41]. Moreover, on these bases one could easily expect that discrepancy may be found between theoretical expectations and experimental results. This problem is common to other nitrides, such as MoN, where from energy band calculations cubic γ-MoN structure is expected to have a $T_c \approx 30$ K. However, this value was not yet achieved probably due to lattice disorder or substoichiometry in nitrogen [25,42]. Finally, it is worth it to underline that in principle NbReN may preserve the possible noncentrosymmetric crystal structure of NbRe and this may also have important consequences on the nature of the superconducting order parameter [21,28].

The depression of T_c with the decrease of the film thickness is often described within the Simonin model [43], by introducing a new boundary condition for the superconducting order parameter in the Ginzburg-Landau (GL) equation. Here the following dependence was derived: $T_c = T_c^b(1\text{-}d_{cr}/d)$, where T_c^b is the critical temperature of the bulk superconductor and d_{cr} is the critical thickness below which $T_c = 0$. The result of the fitting procedure of the $T_c(d_{\mathrm{NbReN}})$ data is reported in Fig. 3(b) as a thick red line by using the parameters $T_c^b = 5.8 \pm 0.1$ K and $d_{cr} = 2.2 \pm 0.1$ nm. As already noticed, the bulk critical temperature is lower compared to the ones estimated for NbRe of about 7.43 K [21]. On the contrary,

$d_{cr} \approx 1$ nm was found in the case of NbRe [21], suggesting a larger coherence length for NbReN, as will be confirmed in the following.

For disordered films the dependence of the critical temperature on the sheet resistance R_S is expected to be more relevant than on the thickness [44]. Therefore, the suppression of T_c as a function of the sheet resistance at $T = 20$ K normalized to the quantum resistance, $R_Q = h/e^2$, was analyzed for the samples of the series 4.5S31, as shown in Fig. 3(c). The strong reduction in T_c for moderate values of R_S/R_Q is typical of homogeneous amorphous disordered compounds, such as WRe and MoGe [44], where both Coulomb interaction and disorder are considered the dominant mechanisms for the T_c suppression. In the framework of the model developed by Finkel'stein for homogeneous amorphous superconductors it is [44,45]

$$\frac{T_c}{T_c^b} = e^{\gamma}\left[\frac{1/\gamma - \sqrt{t/2} + t/4}{1/\gamma + \sqrt{t/2} + t/4}\right]^{1/\sqrt{2t}}, \tag{1}$$

where $t = R_S/\pi R_Q$ and $\gamma = \ln(\hbar/k_B T_c^b \tau)$, with τ the elastic mean free time. The experimental data were compared to the model by leaving T_c^b and γ as free parameters. The result, obtained for $T_c^b = 5.8 \pm 0.1$ K and $\gamma = 7.0 \pm 0.1$, is shown in Fig. 3(c) as a red curve. Despite the scattering of the experimental data, the overall agreement with the theory is satisfactory. The value of the bulk critical temperature is the same as extracted from the Simonin's model, while the large value of γ, which determines the initial slope of the curve, confirms the disordered nature of the samples and is comparable with the numbers obtained for example for TiN [45], NbN [45], and MoSi [12] films. Moreover, from the values of the fitting parameters it is possible to estimate $\tau = 1.2 \times 10^{-15}$ s, as well as the electronic density of states, that for a film 25-nm thick with $\rho_{20} = 160\ \mu\Omega\,\text{cm}$ is $n = me^{-2}/\tau\rho_{20} = 1.8 \times 10^{22}\ \text{cm}^{-3}$ (here m and e are the electron mass and charge, respectively) [46].

In the models of Simonin [43] and Finkel'stein [44] the dependence of the critical temperature on the thickness and sheet resistance is taken into account, respectively. Ivry *et al.* [47] suggested a universal scaling law for T_c as a function of both d and R_S, which could be applied for studying different class of superconductors, from clean to dirty or granular. In particular, the relationship among the different parameters reads as [47]

$$T_c \cdot d = A R_S^{-B}, \tag{2}$$

where A and B are fitting parameters. Interestingly, it was demonstrated [47] that for all the materials reported in the literature the values of the two parameters are correlated, namely Log(A) follows a linear dependence on B. Moreover, their values can provide information concerning the transport mechanism, namely homogeneity or disorder of different kinds of superconductors. For instance, equation (2) was successfully applied to describe the data of homogeneous MoGe films, which results as the material with the largest values of both A and B, almost at the opposite extreme with respect to granular Al [47]. On the contrary, by examining the experimental data of NbN films deposited by different groups, values of B close to the universal exponent $B \approx 1$ were obtained. Figure 3(d) shows the $T_c \cdot d_{\text{NbReN}}(R_S)$ dependence for the samples of the series 4.5S31-d. The red line is the best fit according to Eq. (2) with $A = 109 \pm 38$ (arb. units) and $B = -0.36 \pm 0.08$. Both values are comparable with the fitting parameters derived for granular Al films. Moreover, the two values of A and B satisfactory correlate, as already verified for many superconducting materials. This fit seems to give evidence of a granular nature of the NbReN films. Additional considerations on this point will derive from the forthcoming analysis of the superconducting fluctuations above T_c.

C. Paraconductivity

To study in more detail the role played by the disordered nature of the NbReN films on the superconducting properties, the behavior of the resistive transitions shown in Fig. 3(a) was analyzed in the vicinity of T_c. The evident rounding observed at the onset of the curves can be attributed to the superconducting thermal fluctuations which cause an enhancement of the conductivity with respect to the normal state. This effect has been observed in many superconducting materials [48–51] including granular [52], amorphous [53–56], strongly disordered superconductors [57], and, recently, ultrathin NbN films [58,59]. The fluctuation contribution to the normal-state conductivity above T_c, $\Delta\sigma(T) = \sigma(T) - \sigma_N(T)$ called paraconductivity, was first calculated by Aslamazov and Larkin for the two- (2δ) and three-dimensional (3δ) cases [60] and then extended to one [53,61] and zero dimensions [62]. Here $\sigma(T)$ is the conductivity measured in the absence of magnetic field and $\sigma_N(T)$ is the normal-state conductivity. Depending on the dimensionality δ of the system, $\Delta\sigma(T)$ can be written in a compact form as:

$$\Delta\sigma(T) = \frac{A_\delta}{R_Q}\frac{L^{\delta-3}\xi^{2-\delta}(0)}{\epsilon^{(4-\delta)/2}}, \tag{3}$$

where L is one of the linear dimensions of the superconductor, $\xi(0)$ is the superconducting coherence length at zero temperature, and $\varepsilon \equiv \ln(T/T_c) \approx (T - T_c)/T_c$ is the reduced temperature. δ can be fixed as the number of dimensions in which $L > \xi(T)$ and the values of the numerical factor A_δ are $A_0 = \pi^2/2$, $A_1 = \pi^2/8$, $A_2 = \pi/8$, and $A_3 = \pi/16$. While L represents the film thickness for $\delta = 2$ and L^2 is the cross-sectional area of a superconducting wire for $\delta = 1$, in the case $\delta = 0$ the quantity L^3 can be interpreted as the relevant volume of the sample over which the thermodynamic superconducting fluctuations take place. Moreover, due to the high values of the resistivity of the NbReN films, other contributions to the conductivity (such as, for example, the Maki-Thompson term) [63,64] can be ruled out since they play a predominant role only when the superconductor is in the clean limit [49].

The first sample to be analyzed is 4.5S31-44. Its thickness is much larger than $\xi(0)$, expected to be of the order of the zero-temperature coherence length of NbRe (~5 nm) [21], and therefore the corresponding fluctuations behavior is likely to be 3δ. In Fig. 4(a) the dependence of the measured $\Delta\sigma$ on the reduced temperature ε is reported by closed symbols together with the fit to the experimental data obtained by using Eq. (3) in the case of $\delta = 3$. Since the resistivity of the investigated films is almost constant at low temperatures, we put here (and in all the analyzed films) $\sigma_N(T) = \sigma_N = (\rho_{20})^{-1}$. The comparison between theory and experimental data is

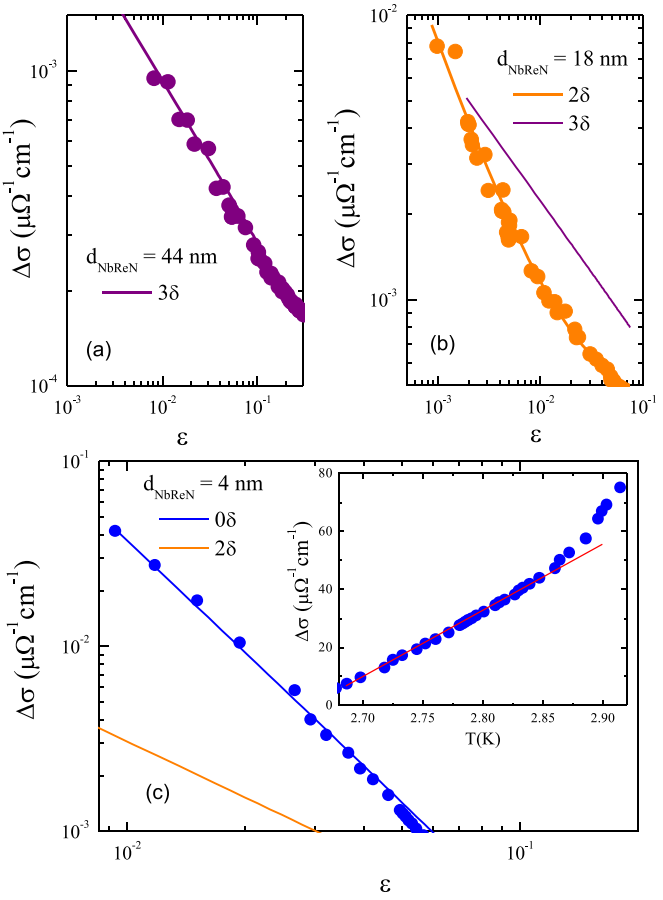

FIG. 4. Dependence of $\Delta\sigma$ on the reduced temperature, ε, for the samples with $d_{\mathrm{NbReN}} = 44$, 18, and 4 nm in panels (a), (b), and (c), respectively. The results of the fitting procedures are obtained by using Eq. (3) in the case of $\delta = 0$, 2, 3 as shown by blue, orange, and purple lines, respectively. In the inset of panel (c) the dependence of $(\Delta\sigma)^{-1/2}$ on the temperature for the sample 4.5S31-4 is shown. The red line is a guide to the eye.

performed fixing $T_c = 5.28$ K (the midpoint of the resistive transition), $\sigma_N = 0.0042$ ($\mu\Omega^{-1}\,\mathrm{cm}^{-1}$) and leaving $\xi(0)$ as the only free parameter. The very nice agreement obtained suggests for this sample a 3δ behavior of the superconducting thermal fluctuations close to T_c and gives $\xi(0) = 4.47 \pm 0.05$ nm, a value very close to that estimated for NbRe [21,22]. When the same procedure is applied to the sample 4.5S31-18 the paraconductivity shows a clear 2δ behavior. The experimental data and the fitting curve, obtained from Eq. (3) in the case of $\delta = 2$, are shown by closed symbols and orange line, respectively, in Fig. 4(b). In this case $T_c = 5.18$ K and $\sigma_N = 0.0077$ ($\mu\Omega^{-1}\,\mathrm{cm}^{-1}$). The film thickness $d = 20.3 \pm 0.3$ nm is obtained as the only free parameter and it is in reasonable agreement with the nominal one. A poor matching of the theory with the experiment is obtained when the data are fitted with the 3δ model. The purple line is the plot of Eq. (3) with $\delta = 3$, the fixed values of T_c and σ_N used above, and the unphysical value $\xi(0) = 0.34 \pm 0.05$ nm. The 2δ behavior of the paraconductivity of this sample can be understood if we consider that at high temperatures, where $\xi(T) = \xi(0)/(1 - T/T_c)^{1/2}$ diverges, a superconducting film always exhibits a 2δ behavior. In fact, along the lines of what have been demonstrated in the case of layered superconductors [65], a 2δ-3δ crossover sets in at the temperature where $\xi(T) \sim d/2$. For the sample 4.5S31-18, by using $\xi(0) = 4.47$ nm, this happens at $T_{2\delta-3\delta} \sim 3.92$ K, a temperature far from T_c being $t_{2\delta-3\delta} = T_{2\delta-3\delta}/T_c \sim 0.76$. On the contrary, the sample 4.5S31-44 is always in the 3δ regime since in this case $T_{2\delta-3\delta} \sim 5.05$ K and $t_{2\delta-3\delta} \sim 0.96$. Interesting results are found when the above analysis is performed for the thinnest samples of the series which show a ε^{-2} dependence of the paraconductivity. As can be seen from Eq. (3) this corresponds to a 0δ nature of the fluctuations and has already been observed in planar arrays of nanoparticles [62], in granular superconductors [59,66,67], and also in polymeric superconductors where, due to the peculiar nature of this system, a 1δ behavior has also been reported [61]. In Fig. 4(c) the temperature dependence of $\Delta\sigma$ is shown for the sample 4.5S31-4. The fit to the experimental data has been done using Eq. (3) for the case $\delta = 0$. $T_c = 2.67$ K, $\sigma_N = 0.0072$ ($\mu\Omega^{-1}\,\mathrm{cm}^{-1}$), and $\xi(0) = 4.47$ nm have been kept fixed during the procedure and the volume of the fluctuation domain L^3 has been set equal to $d \cdot l_{fd}^2$, where l_{fd} is the fluctuation domain length, namely the length over which fluctuations take place. In this way the length l_{fd} remains the only free parameter. For this sample it is $l_{fd} = 49 \pm 2$ nm and the fit is presented in Fig. 4(c) as a blue line. The orange line is the behavior of the paraconductivity calculated for $\delta = 2$, by leaving T_c, σ_N, and d as free fitting parameters. Despite that the values obtained for these quantities are all reasonable [$T_c = 2.67 \pm 0.01$ K, $\sigma_N = 0.0074 \pm 0.0002$ ($\mu\Omega^{-1}\,\mathrm{cm}^{-1}$), $d = 4.9 \pm 0.3$ nm], the discrepancy of the 2δ theoretical prediction with the experimental data is evident. Similar values for l_{fd} have been obtained for the samples 4.5S31-6, 4.5S31-9 [not shown in Fig. 3(a)], and 4.5S31-13. In the inset of Fig. 4(c) the inverse square root of $\Delta\sigma$ as a function of the temperature for the sample 4.5S31-4 is shown. The linearity of the curve extends from 2.69 to 2.86 K, while above this temperature the measurements lay above the red line. If the data between 2.86 and 2.93 K were shown in a $(\Delta\sigma)^{-1}$ vs T plot, they would follow a linear behavior. In fact, when the temperature approaches T_c the coherence length diverges becoming larger than l_{fd} and the superconducting fluctuations change from a 0δ to a 2δ nature. For the sample 4.5S31-44, considering $\xi(0) = 4.47$ nm, this 0δ-2δ crossover happens at a temperature $\sim 0.98\,T_c$. The behavior shown by the ultrathin NbReN films is very similar to what was observed in granular superconductors and ascribed to a possible Josephson coupling among the grains [59,62,66,67]. On the contrary, the experimental results are different from what observed in amorphous bismuth films 10-nm thick (for which a value of 6.5 nm was estimated for ξ at zero temperature) where was reported a ε^{-1} dependence of $\Delta\sigma$, a signature of the 2δ nature of the superconducting fluctuations [54–56]. It emerges that, similarly to what was recently reported for NbN ultrathin films [59], it is l_{fd} the effective length over which the 0δ fluctuations develop. This result supports the picture of a structure made of small crystallites, smaller than l_{fd}.

D. NbReN bridges

In this section the electric transport measurements performed on structured films are reported. At this purpose, the

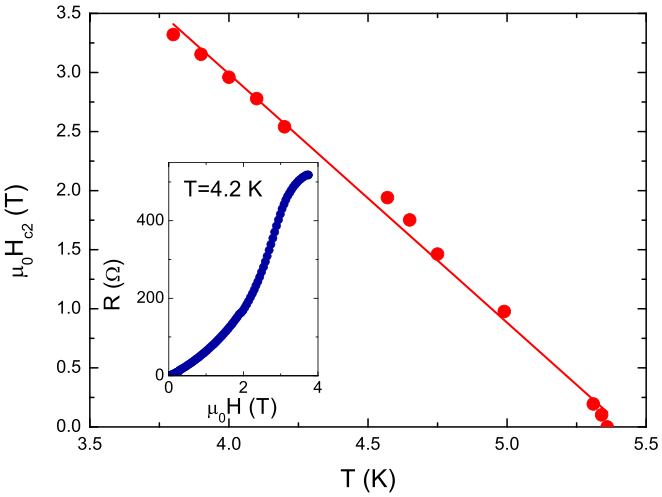

FIG. 5. Temperature dependence of the perpendicular upper critical magnetic field for the patterned film 45S33. The red line is a linear fit of the experimental data. Inset: dependence of electrical resistance on the magnetic field, $R(H)$, at $T = 4.2$ K.

samples were patterned into a Hall bar geometry of width $w = 10\ \mu$m and distance between the voltage contacts $\Lambda = 90\ \mu$m. In order to evaluate the temperature dependence of the perpendicular upper critical field, $\mu_0 H_{c2}$, resistance as a function of the magnetic field, $R(H)$, measurements at fixed values of the temperature [see Fig. 5(a)] and $R(T)$ measurements at fixed values of H were performed with H applied perpendicularly to the substrate plane and with a bias current of $I_b = 100\ \mu$A. $\mu_0 H_{c2}$ was defined also in this case at 90% of the normal state resistance. In Fig. 5(b) the (H, T) phase diagram of the 45S33 film is shown. A typical $R(H)$ transition curve measured at $T = 4.2$ K is reported in the inset of Fig. 5(a).

$\mu_0 H_{c2}$ follows a linear temperature dependence, which was fitted in the overall temperature range to determine the value of $\mu_0 H_{c2}(0) = 11.4\ \pm 0.2$ T, much larger than the ones measured for Nb and slightly lower than in NbRe. Since $\mu_0 H_{c2}(0) = \Phi_0/[2\pi\xi(0)^2]$, where $\Phi_0 = 2.07 \times 10^{-15}$ Wb is the flux quantum [68], the parallel GL coherence length at zero temperature, $\xi(0)$, can be evaluated. It is $\xi(0) = 5.40 \pm 0.08$ nm, larger (lower) with respect to NbRe (Nb) [21,69]. It is now possible to compare the value of the coherence length with the one extracted from the analysis of the superconducting fluctuation, from which $\xi(0)$ was slightly underestimated.

Moreover, from the slope of the $\mu_0 H_{c2}(T)$ curve the value of the quasiparticle (qp) diffusion coefficient D can be estimated [70], since $D = (4k_B/\pi e) \times (\mu_0 dH_{c2}/dT|_{T=T_c})^{-1} = 0.52 \pm 0.01 \times 10^{-4}\ \ m^2/s$, with $(\mu_0 dH_{c2}/dT|_{T=T_c}) = -2.10 \pm 0.05$ T/K. The value of D is comparable with NbN [58,71], NbRe [22], as well as amorphous WSi [72]. It follows, in turn, that the mean free path $l = (3D\tau)^{1/2} \approx 0.5$ nm [58]. Moreover, from the value of $T_c = 5.36$ K and of the low temperature resistivity $\rho_{20} = 224\ \mu\Omega$ cm it is possible to derive the magnetic penetration depth at zero temperature from the relation [73] $\lambda(0) = 1.05 \times 10^{-3}(\rho_{20}/T_c)^{0.5} = 679$ nm. Therefore the GL parameter is $\kappa = \lambda/\xi = 126$ and the lower critical field $\mu_0 H_{c1}(0) = (\Phi_0/4\pi\lambda^2)\ln\kappa = 1.7$ mT [74]. Furthermore, the density of states at the Fermi level was estimated by using the free-electron Einstein's relation [75] $N_0 = 1/(e^2\rho_n D) = 3.4 \times 10^{47}\ \ J^{-1}m^{-3}$. The value of N_0, crucial for determining the performance of a SNSPD as will be clear in the following, is comparable with NbRe [21]. Finally, the value of the superconducting energy gap at $T = 0$ can be evaluated according to the relation $\Delta(0) = \hbar\rho_{20}/\lambda(0)^2\pi\mu_0$ valid in the dirty limit [75]. It results that $\Delta(0) = 0.8$ meV, namely reduced by about 20% with respect to NbRe and comparable to WSi films [1,21,72].

Voltage-current $V(I)$ characteristics were measured both as a function of the temperature and of the perpendicular applied magnetic field on the film 45S33. The curves were recorded by current biasing the bridge with a pulsed current (current-on time 12 ms, current-off time 1 s), and the critical current I_c is defined by using a $V_c = 40$ mV/m criterion. In this way the critical current density, $J_c = I_c/wd_{NbReN}$, was estimated. The sample has $J_c = 7.4 \times 10^9\ \ A/m^2$ at a reduced temperature $t = T/T_c \approx 0.5$ and in zero field, a value comparable with NbRe bridges [22]. In Fig. 6(a) a selection of $V(I)$ characteristics for different H values at $T = 4.2$ K are shown, while the magnetic field dependence of J_c at this temperature is shown in panel (b). From the comparison between the $J_c(H)$ dependence for the NbReN sample under study and a single NbRe film of Ref. [22] at $t \approx 0.5$, reported in the inset of the same figure, it results that the values of the critical current densities for the two systems are comparable. On the contrary, J_c is intermediate between the two classes of materials, namely lower (larger) than crystalline nitrides [58,71] (amorphous [12,14]) superconductors.

It is also useful to compare J_c with the expected value of the depairing current density J_{dp}, which is the intrinsic critical current the material can support. The values of J_{dp} at $T = 0$ are evaluated according to $J_{dp}(0) = (8\pi^2\sqrt{2\pi}/21\zeta(3)e) \times \sqrt{(k_B T_c)^3/\hbar v_F \rho(\rho l)}$ [76], where only microscopic experimental parameters are present and ζ is the Riemann zeta function. It results that $J_{dp}(0) \approx 9.4 \times 10^{10}\ \ A/m^2$. The comparison between J_{dp} with the measured critical current density values at the same t can be obtained by using the universal form of $(J_{dp}(t)/J_{dp}(0))^{2/3}$ vs t given by the theory of Kupriyanov and Lukichev via numerical solution [77]. At $t = 0.5$ it is $J_c/J_{dp} \approx 0.3$, smaller than that reported for NbRe, where, however, meanders made of nanowires from 50- to 100-nm wide and 8-nm thick were measured [23].

The last point concerns the pinning mechanism present in the 45S33 film, and this study is relevant since it is well established that vortices may play an important role in the detection mechanism in SNSPDs [72]. The pinning properties of a material depend on both magnetic field and temperature, but they also are linked to the microscopical structure of the sample [78,79]. Since a particular scaling law is characteristic of a specific pinning mechanism, it is useful to plot the reduced pinning force, $f_p = F_p/F_p^{max}$, as a function of a reduced magnetic field, $h = H/H^*$, at different temperatures, as reported in Fig. 6(c). Here the measured pinning force is given by $F_p = J_c \cdot \mu_0 H$, F_p^{max} is the maximum pinning force at each temperature, while $\mu_0 H^*$ is defined as the field at which the sample resistance is 1% of R_{max}, evaluated from $R(H)$ measurements at different temperatures. The normalization with respect to fields lower than $\mu_0 H_{c2}$ is common

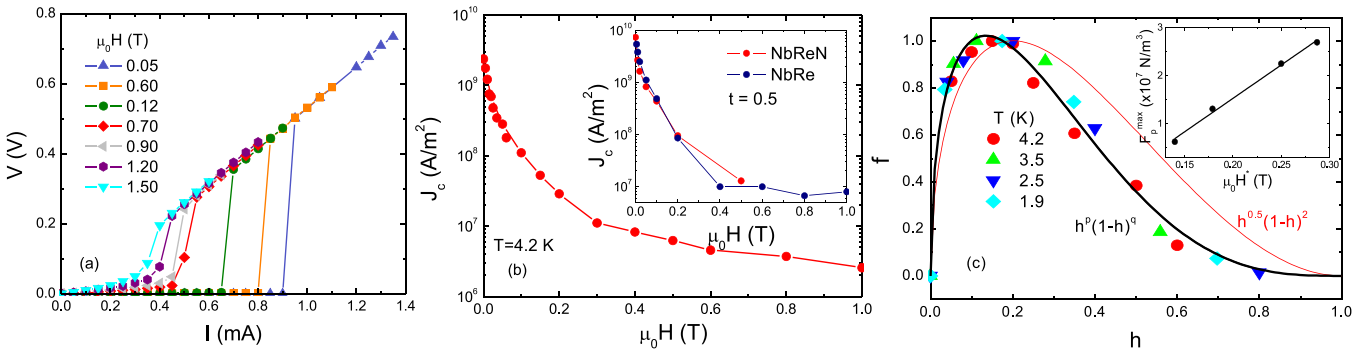

FIG. 6. (a) Representative of $V(I)$ characteristics, measured at $T = 4.2$ K, as a function of the applied magnetic field. (b) Magnetic field dependence of the critical current density at $T = 4.2$ K. Inset: comparison between the $J_c(\mu_0 H)$ dependence for NbRe (blue points) and NbReN (red points) films at $t = 0.5$. (c) Scaling of the normalized pinning force as a function of the reduced magnetic field. The lines correspond to the $f_p \propto h^p(1-h)^q$ dependence for $p = 0.5$ and $q = 2$ (thin red line) and $p = 0.47$ and $q = 3$ (thick black line). Inset: dependence of the maximum pinning force at each temperature as a function of $\mu_0 H^*$. The line is a guide to the eyes. All the data refer to the patterned film 45S33.

for many superconductors, with $\mu_0 H^*$ often representing the field at which either the magnetic irreversibility or J_c go to zero [80,81]. The current choice for $\mu_0 H^*$ is proved here by the linear dependence of F_p^{max} on $\mu_0 H^*$ reported in the inset of Fig. 6(c). The clear scaling behavior of Fig. 6(c) can be analyzed considering the general law $f_p \propto h^p(1-h)^q$, where the values of p and q determine the details of the pinning mechanism. The flux-line shear (FLS) model ($p = 0.5$ and $q = 2$), valid for the motion of the flux lines along weak-pinning percolative paths, is shown as a red line in Fig. 6(c). This model does not describe the experimental data, which present a narrower distribution and a smearing at large h. For this reason, a best fitting procedure was performed which resulted in $p = 0.47 \pm 0.04$ and $q = 3.0 \pm 0.2$, as displayed by a thick black line in the figure. In accordance with this modeling, the position of the maximum reduced pinning force, f_p^{max} expected at $h_p^{max} = p/(p+q) = 0.143 \pm 0.03$, is indeed observed at 0.135. As reported in the literature a value of q larger than 2 may indicate the presence of dishomogeneities which can be modeled as a distribution of the channel properties [79,82]. This behavior, common to many classes of superconducting materials [80,81], seems appropriate in the case of disordered NbReN films.

The $V(I)$ data in the presence of perpendicular field were also analyzed in the framework of the theory of Larkin and Ovchinnikov (LO) [83], which provides convenient access to the estimation of the lifetimes of electronic excitations in superconductors, τ_E. This approach, alternative to optical pump-and-probe experiments, is widely used to gain information about the time performance of candidate materials for fast SNSPDs or NbN bridges [18,71,84,85], since it is well established that the scaling between the values extracted within the vortex instability approach and from optical experiments is solid [18]. According to the model of LO, at small magnetic fields it is possible to correlate the sudden jump at a current value I^* and at a critical voltage V^* to the vortex instability occurring for $V^* = \mu_0 v^* H L$ [86]. The qp relaxation time is then linked to v^* by the expression $v^* = D^{1/2}[14\zeta(3)]^{1/4}(1-t)^{1/4}/(\pi\tau_E)^{1/2}$ [86]. The inset of Fig. 7(a) shows a representative of $V(I)$ curves in the low

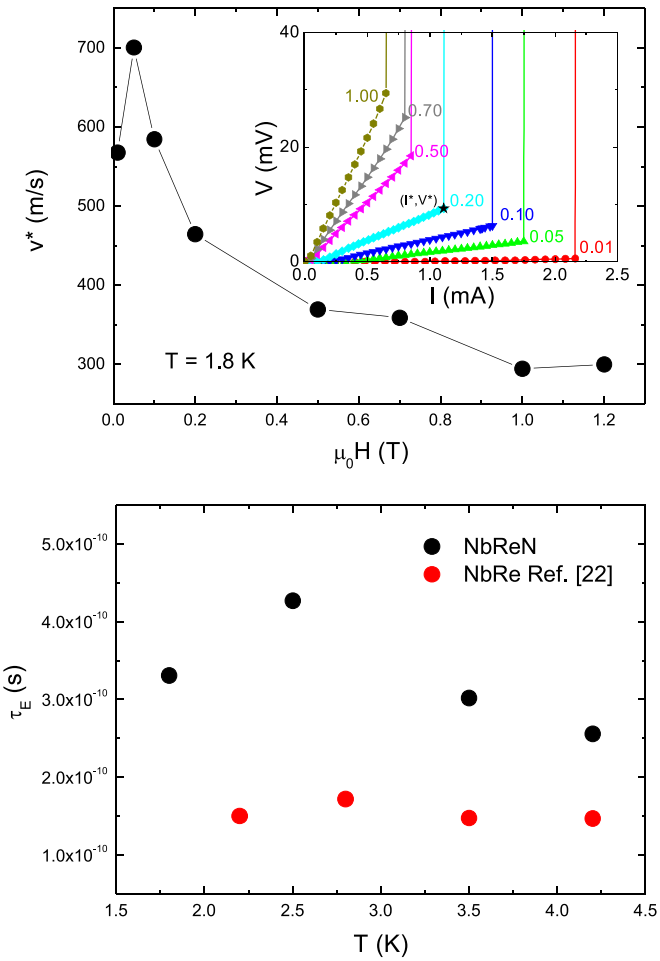

FIG. 7. (a) v^* as a function of the applied magnetic field at $T = 1.8$ K. Inset: Representative of $V(I)$ characteristics in the low-voltage region, measured at $T = 1.8$ K, as a function of $\mu_0 H$ (expressed in T in the labels). The current and voltage at which instability occurs are indicated as I^* and V^*, respectively. (b) Temperature dependence of the qp relaxation times for NbReN and NbRe [22] bridges evaluated at $\mu_0 H = 0.5$ and 0.6 T, respectively. All the data refer to the patterned film 45S33.

TABLE II. Values of the parameters which characterize the 45S33 patterned film 36-nm thick, as extracted from $R(H)$, $R(T)$, and $V(I)$ curves, compared to the ones estimated for NbRe films [21,22].

Parameters	NbReN	NbRe
T_c (K)	5.36	7.30
ρ_{20} ($\mu\Omega$ cm)	224	143
$\mu_0 H_{c1}(0)$ (mT)	1.7	3.4
$\mu_0 H_{c2}(0)$ (T)	11.4	14.4
D ($\times 10^{-4}$ m^2/s)	0.52	0.56
$\xi(0)$ (nm)	5.40	4.80
$\lambda(0)$ (nm)	679	472
$N_0 \times 10^{47}$ (J^{-1} m^{-3})	3.4	4.8
$\Delta(0)$ (meV)	0.8	1.1
τ_E (ps)	300	200

voltage regime measured for the bridge 45S33 under perpendicular fields from $\mu_0 H = 0.01$ to 1.00 T at $T = 1.8$ K. As an example, the occurrence of the instability is indicated as (I^*, V^*) for $\mu_0 H = 0.20$ T. The resulting field dependence of v^*, with the characteristic peak at low $\mu_0 H$ [87], is reported in the main panel of Fig. 7(a). The same analysis was performed at different temperatures, in such a way to obtain the $\tau_E(T)$ dependence, as shown in Fig. 7(b) for $\mu_0 H = 0.5$ T. It results that τ_E smoothly depends on T and that $\tau_E^{\mathrm{NbReN}} \approx 300$ ps. As a comparison in Fig. 7(b) the same dependence for the case of a NbRe bridge 15-nm thick for $\mu_0 H = 0.6$ T is reported. While it is evident that NbRe is about 70% faster than NbReN (but this may be due also to the thickness difference [88]), it is also worth noticing that τ_E^{NbReN} is still about one order of magnitude smaller than the value reported in literature for NbN [71,84,89]. However, to obtain a better insight into the time performance of real devices, a more systematic study on new ultrathin films structured in narrower bridges will be the subject of future studies. Both the low values of $\tau_E(T)$ and its weak temperature dependence are desirable in the design of SNSPD. In particular, since small $\tau_E(T)$ may result in short recovery times, it is reasonable to expect that a possible NbReN-based device may be characterized by fast dynamics. The main parameters derived for the investigated film are summarized in Table II.

IV. DISCUSSION

The transport properties shown in the previous sections reveal that NbReN is a dirty superconductor, being $l \ll \xi(0)$. Moreover, the high resistivity values and $RRR < 1$ seem to suggest that the NbReN films are disordered. The level of disorder can be characterized by the Ioffe-Regel (IR) parameter [90], $k_F l = 3Dm/\hbar$ where k_F is the Fermi wave vector. According to the IR criterion the metal-insulator transition (MIT) occurs when $k_F l = 3Dm/\hbar \leqslant 1$. In the case of the film 45S33, it can be estimated that $k_F l = 3Dm/\hbar \approx 1.3$, lower compared to amorphous MoSi films [12,91], and close to the MIT threshold value. Further analysis of the $R(T)$ data (not shown here) seems to exclude hopping as the main conduction mechanism, while it is reasonable to suppose that disorder and grain boundary scattering play a crucial role [91]. These observations are consistent with the results emerging from the XRD measurements shown in Fig. 1, namely a samples' morphology made of crystallites of small dimensions and different orientations. In the following the discussion focuses on the analysis of the material's parameters which are relevant for the application of NbReN in the field of superconducting electronics. First, the suitability of this material for single photon detection will be analyzed, starting with a detailed comparison with other superconductors as well as with NbRe to verify if NbReN could in principle represent a significant improvement in terms of some specific figures of merit with respect to its parent material [23]. The expected features of a possible NbReN-based device will in fact depend on some intrinsic material properties that were estimated in this work [1]. The first observation concerns the small values of T_c (and consequently Δ), by far lower than for standard nitrides (NbN, NbTiN) [5] and comparable with amorphous WSi [72,92] or NbSi [14], which could make the material appealing for detecting low energy photons for application in the quantum communication frequency range. Indeed, in the framework of the normal conducting hot-spot model [93], the minimum photon energy detectable by the device, E_{min}, can be expressed as $E_{\mathrm{min}} \propto N_0 \Delta^2 w d (D\tau_{\mathrm{th}})^{1/2}(1 - I_b/I_c)$ [94]. Even if this formula represents an oversimplification, it is intuitively understandable, and it gives evidence for the fact that low values of both Δ and N_0 may be the reason of the unprecedented high values of the quantum efficiency shown by amorphous superconductors, such as WSi [10,95] or NbSi [14], which are all highly resistive materials. This expression is also useful to compare the possible performance of NbReN-based detectors with NbRe [21–23]. It results that, for the same film geometry, E_{min} is two times smaller in the case of NbReN. In particular, by considering that for NbRe SNSPDs a saturated internal efficiency up to $\lambda = 1.3$ μm was measured, an extension of the operation frequency of $\lambda = 2$ μm NbReN can be predicted. This may have a significant impact for applications as Light detection and Ranging (LIDAR) and satellite communications [96–98]. The dimension of the hot spot should also be considered in this analysis. The maximum HS radius roughly scales with the microscopical parameters as $r_{\mathrm{max}} \propto (E_{\mathrm{ph}}/\Delta^2 N_0 d D\tau_{\mathrm{th}})^{1/2}(1/N_0\Delta)^{1/3}$, where E_{ph} is the photon energy [99]. Again, by comparing NbReN and NbRe for the same film geometry and photon energy, it results that r_{max} is 60% larger for the new material, a feature which could simplify the challenge of extreme pattering. Moreover, the structure made of small crystallites can be advantageous for the substrate choice or the films structuring. Finally, it is worth commenting on the reduced values of the superconducting coherence length (again intermediate between Nb [58,71] and WSi [72] for instance) which is desirable for the realization of devices based ultrathin films without a dramatic T_c reduction. In summary, the auspice is that compared to the encouraging results obtained for NbRe [23], NbReN may show a substantial gain in terms of efficiency, while preserving the good time performance of the parent material NbRe. If detection experiments will confirm these expected performances, the employment of NbReN in the field of single photon detectors could open the way to the implementation of devices with promising performances also in the growing field of quantum communication.

In addition, the possibility of application of NbReN films for the realization of kinetic inductance detectors (KIDs) [100] could also be considered. In fact, the disorder-dominated transport properties, the granular morphology, as well as the reduced T_c are all desirable characteristics at this purpose. By estimating the sheet kinetic inductance for the sample 45S33 it results that $L_{k,S} = \hbar\rho_n/\pi\Delta d = 16$ pH/square, a value comparable with the ones reported in literature for other disordered thin films of metallic compounds or granular Al [101].

Finally, it is worth commenting about the interest in the fundamental investigation of this material. In particular, experiments aiming at accessing both the value and the nature of the superconducting gap by spectroscopic techniques will be performed. Since NbReN originates from a material lacking the inversion symmetry in its crystal structure, in principle the possible presence of exotic pairing cannot be excluded. However, in order to perform reliable experiments in this sense films with better crystallographic properties are required.

V. CONCLUSIONS

Superconducting NbReN thin films were deposited by reactive dc sputtering. The deposition conditions were tuned in order to maximize T_c, which, however, at this stage is still lower than NbRe, recently suggested as a valuable candidate for the realization of fast SNSPDs [22,23]. This result may be related to its disordered nature, as confirmed by preliminary XRD analysis which indicate that the films are moderately textured. Electrical transport measurements were performed and the main microscopical parameters of the material were estimated. In order to gain insight in the conduction mechanisms in NbReN films, different scaling behaviors of the critical temperature were considered. On the basis of these findings the suitability of NbReN for the future realization of single photon detectors was discussed. These results indicate that the synthesis of this disordered superconductor provides a promising platform for research in the field of SNSPDs.

ACKNOWLEDGMENTS

The authors are grateful to Iman Esmaeil Zadeh for inspiring this work and to Serghej Prischepa for useful discussions. This research was partially supported by both the National Operative Programme for Companies and Competitiveness 2014-2020 - Horizon 2020, funded by the European Union (Rilub SPA, project leader. Project no. F/050190/01-02/x32 - INNOLUBE) and by the National Operative Programme for Research and Innovation 2014-2020, funded by the European Union (FATER spa, project leader. ARS01_01088 - RINASCIMENTO). A.d.B. acknowledges funding from the Alexander von Humboldt Foundation in the framework of a Sofja Kovalevskaja award endowed by the German Federal Ministry of Education and Research.

[1] I. Holzman and Y. Yachin, Superconducting nanowires for single-photon detection: progress, challenges, and opportunities, Adv. Quantum Technol. **2**, 1800058 (2019).

[2] C. M. Natarajan, M. G. Tanner, and R. H. Hadfield, Superconducting nanowire single-photon detectors: physics and applications, Supercond. Sci. Technol. **25**, 063001 (2012).

[3] H. Zhang, L. Xiao, B. Luo, J. Guo, L. Zhang, and J. Xie, The potential and challenges of time-resolved single-photon detection based on current-carrying superconducting nanowires, J. Phys. D: Appl. Phys. **53**, 013001 (2020).

[4] W. Zhang, Q. Jia, L. You, X. Ou, H. Huang, L. Zhang, H. Li, Z. Wang, and X. Xie, Saturating intrinsic detection efficiency of superconducting nanowire single-photon detectors via defect engineering, Phys. Rev. Appl. **12**, 044040 (2019).

[5] X. Yang, L. You, L. Zhang, C. Lv, H. Li, X. Liu, H. Zhou, and Z. Wang, Comparison of superconducting nanowire single-photon detectors made of NbTiN and NbN thin films, IEEE Trans. Appl. Supercond. **28**, 2200106 (2018).

[6] J. Zichi, J. Chang, S. Steinhauer, K. V. Fieandt, J. W. N. Los, G. Visser, N. Kalhor, T. Lettner, A. W. Elshaari, I. E. Zadeh, and V. Zwiller, Optimizing the stoichiometry of ultrathin NbTiN films for high-performance superconducting nanowire single-photon detectors, Opt. Express **27**, 26579 (2019).

[7] C. J. K. Richardson, A. Alexander, C. G. Weddle, B. Arey, and M. Olszta, Low-loss superconducting titanium nitride grown using plasma-assisted molecular beam epitaxy, J. Appl. Phys. **127**, 235302 (2020).

[8] J. Wright, C. Chang, D. Waters, F. Lüpke, L. Raymond, R. Koscica, G. Khalsa, R. Feenstra, D. Muller, H. G. Xing, and D. Jena, An unexplored MBE growth mode reveals new properties of superconducting NbN, Phys. Rev. Materials **5**, 024802 (2021).

[9] T. Polakovic, S. Lendinez, J. E. Pearson, A. Hoffmann, V. Yefremenko, C. L. Chang, W. Armstrong, K. Hafidi, G. Karapetrov, and V. Novosad, Room temperature deposition of superconducting niobium nitride films by ion beam assisted sputtering, APL Mater. **6**, 076107 (2018).

[10] F. Marsili, V. B. Verma, J. A. Stern, S. Harrington, A. E. Lita, T. Gerrits, I. Vayshenker, B. Baek, M. D. Shaw, R. P. Mirin, and S. W. Nam, Detecting single infrared photons with 93% system efficiency, Nat. Photonics **7**, 210 (2013).

[11] V. B. Verma, A. E. Lita, M. R. Vissers, F. Marsili, D. P. Pappas, R. P. Mirin, and S. W. Nam, Superconducting nanowire single photon detectors fabricated from an amorphous $Mo_{0.75}Ge_{0.25}$ thin film, Appl. Phys. Lett. **105**, 022602 (2014).

[12] A. Banerjee, L. J. Baker, A. Doye, M. Nord, R. M. Heath, K. Erotokritou, D. Bosworth, Z. H. Barber, I. MacLaren, and R. H. Hadfield, Characterization of amorphous molybdenum silicide (MoSi) superconducting thin films and nanowires, Supercond. Sci. Technol. **30**, 084010 (2017).

[13] Y. Korneeva, N. Manova, I. Florya, M. Mikhailov, O. V. Dobrovolskiy, A. A. Korneev, and D. Yu. Vodolazov, Different single-photon response of wide and narrow superconducting Mo_xSi_{1-x} strips, Phys. Rev. Appl. **13**, 024011 (2020).

[14] S. N. Dorenbos, P. Forn-Diaz, T. Fuse, A. H. Verbruggen, T. Zijlstra, T. M. Klapwijk, and V. Zwiller, Low gap superconducting single photon detectors for infrared sensitivity, Appl. Phys. Lett. **98**, 251102 (2011).

[15] L. You, Superconducting nanowire single-photon detectors for quantum information, Nanophotonics **9**, 2673 (2020).

[16] H. Shibata, T. Akazaki, and Y. Tokura, Fabrication of MgB_2 nanowire single-photon detector with meander structure, Appl. Phys. Express **6**, 023101 (2011).

[17] H. Y. Tong, H. L. Zhang, Z. Z. Hui, X. W. Tang, R. H. Wei, W. H. Song, L. Hu, C. B. Cai, X. B. Zhu, and Y. P. Sun, Epitaxial superconducting δ-MoN and δ-NbN thin films by a chemical solution deposition, J. Alloys Compd. **826**, 154231 (2020).

[18] O. V. Dobrovolskiy, D. Yu. Vodolazov, F. Porrati, R. Sachser, V. M. Bevz, M. Yu. Mikhailov, A. V. Chumak, and M. Huth, Ultra-fast vortex motion in a direct-write Nb-C superconductor, Nat. Commun. **11**, 3291 (2020).

[19] R. Arpaia, M. Ejrnaes, L. Parlato, F. Tafuri, R. Cristiano, D. Golubev, R. Sobolewski, T. Bauch, F. Lombardi, and G. P. Pepe, High-temperature superconducting nanowires for photon detection, Physica C **509**, 16 (2015).

[20] G. J. Orchin, D. De Fazio, A. Di Bernardo, M. Hamer, D. Yoon, A. R. Cadore, I. Goykhman, K. Watanabe, T. Taniguchi, J. W. A. Robinson, R. V. Gorbachev, A. C. Ferrari, and R. H. Hadfield, Niobium diselenide superconducting photodetectors, Appl. Phys. Lett. **114**, 251103 (2019).

[21] C. Cirillo, G. Carapella, M. Salvato, R. Arpaia, M. Caputo, and C. Attanasio, Superconducting properties of noncentrosymmetric $Nb_{0.18}Re_{0.82}$ thin films probed by transport and tunneling experiments, Phys. Rev. B **94**, 104512 (2016).

[22] M. Caputo, C. Cirillo, and C. Attanasio, NbRe as candidate material for fast single photon detection, Appl. Phys. Lett. **111**, 192601 (2017).

[23] C. Cirillo, J. Chang, M. Caputo, J. W. N. Los, S. Dorenbos, I. Esmaeil Zadeh, and C. Attanasio, Superconducting nanowire single photon detectors based on disordered NbRe films, Appl. Phys. Lett. **117**, 172602 (2020).

[24] R. S. Ningthoujam and N. S. Gajbhiye, Synthesis, electron transport properties of transition metal nitrides and applications, Prog. Mater. Sci. **70**, 50 (2015).

[25] D. A. Papaconstantopoulos, W. E. Pickett, B. M. Klein, and L. L. Boyer, Nitride offers 30 K transition?, Nature (London) **308**, 494 (1984).

[26] D. Jena, R. Page, J. Casamento, P. Dang, J. Singhal, Z. Zhang, J. Wright, G. Khalsa, Y. Cho, and H. G. Xing, The new nitrides: layered, ferroelectric, magnetic, metallic and superconducting nitrides to boost the GaN photonics and electronics eco-system, Jpn. J. Appl. Phys. **58**, SC0801 (2019).

[27] A. G. Knapton, The niobium-rhenium system, J. Less-Common Met. **58**, 480 (1959).

[28] E. Bauer and M. Sigrist, *Non-Centrosymmetric Superconductors: Introduction and Overview* (Springer, London, 2012).

[29] D. D. Bacon, A. T. English, S. Nakahara, F. G. Peters, H. Schreiber, W. R. Sinclair, and R. B. van Dover, Properties of NbN thin films deposited on ambient temperature substrates, J. Appl. Phys. **54**, 6509 (1983).

[30] D. M. Glowacka, D. J. Goldie, S. Withington, H. Muhammad, G. Yassin, and B. K. Tan, Development of a NbN deposition process for superconducting quantum sensors, arXiv:1401.2292.

[31] B. G. C. Bos, D. J. Thoen, E. A. F. Haalebos, P. M. L. Gimbel, T. M. Klapwijk, J. J. A. Baselmans, and A. Endo, Reactive magnetron sputter deposition of superconducting Niobium Nitride thin films with different target sizes, IEEE Trans. Appl. Supercond. **27**, 1500405 (2017).

[32] Z. Wang, A. Kawakami, Y. Uzawa, and B. Komiyama, Superconducting properties and crystal structures of single-crystal Niobium Nitride thin films deposited at ambient substrate temperature, J. Appl. Phys. **79**, 7837 (1998).

[33] L. J. van der Pauw, A method of measuring specific resistivity and Hall effect of discs of arbitrary shape, Philips Res. Rep. **13**, 1 (1958).

[34] C. S. Lue, T. H. Su, H. F. Liu, and B.-L. Young, Evidence for s-wave superconductivity in noncentrosymmetric $Re_{24}Nb_5$ from ^{93}Nb NMR measurements, Phys. Rev. B **84**, 052509 (2011).

[35] J. Chen, L. Jiao, J. L. Zhang, Y. Chen, L. Yang, M. Nicklas, F. Steglich, and H. Q. Yuan, BCS-like superconductivity in the noncentrosymmetric compounds Nb_xRe_{1-x} ($0.13 \leqslant x \leqslant 0.38$), Phys. Rev. B **88**, 144510 (2013).

[36] A. L. Patterson, The Scherrer Formula for X-Ray Particle Size Determination, Phys. Rev. **56**, 978 (1939).

[37] M. Ohring, *Materials Science of Thin Films* (Academic Press, London, 1992).

[38] J. H. Tyan and J. T. Lue, Grain boundary scattering in the normal state resistivity of superconducting NbN thin films, J. Appl. Phys. **75**, 325 (1994).

[39] P. Patsalas, N. Kalfagiannis, S. Kassavetis, G. Abadias, D. V. Bellas, Ch. Lekka, and E. Lidorikis, Conductive nitrides: growth principles, optical and electronic properties, and their perspectives in photonics and plasmonics, Mater. Sci. Eng., R **123**, 1 (2018).

[40] M. J. Winiarski, Electronic structure of non-centrosymmetric superconductors $Re_{24}(NbTi)_5$ by ab initio calculations, J. Alloys Compd. **616**, 1 (2014).

[41] S. K. Ghosh, M. Smidman, T. Shang, J. F. Annett, A. Hillier, J. Quintanilla, and H. Yuan, Recent progress on superconductors with time-reversal symmetry breaking, J. Phys.: Condens. Matter **33**, 033001 (2021).

[42] S. Wang, D. Antonio, X. Yu, J. Zhang, A. L. Cornelius, D. He, and Y. Zhao, The hardest superconducting metal nitride, Sci. Rep. **5**, 13733 (2015).

[43] J. Simonin, Surface term in the superconductive Ginzburg-Landau free energy: Application to thin films, Phys. Rev. B **33**, 7830(R) (1986).

[44] A. M. Finkel'stein, Suppression of superconductivity in homogeneously disordered systems, Physica B **197**, 636 (1994).

[45] N. Hadacek, M. Sanquer, and J.-C. Villéegier, Double reentrant superconductor-insulator transition in thin TiN films, Phys. Rev. B **69**, 024505 (2004).

[46] N. W. Ashcroft and N. D. Mermin, *Solid State Physics* (Saunders College, Philadelphia, 1976).

[47] Y. Ivry, C.-S. Kim, A. E. Dane, D. De Fazio, A. N. McCaughan, K. A. Sunter, Q. Zhao, and K. K. Berggren, Universal scaling of the critical temperature for thin films near the superconducting-to-insulating transition, Phys. Rev. B **90**, 214515 (2014).

[48] G. Balestrino, A. Nigro, R. Vaglio, and M. Marinelli, Thermodynamic fluctuations in the 110-K Bi-Sr-Ca-Cu-O superconductor: Evidence for two-dimensional behavior, Phys. Rev. B **39**, 12264 (1989).

[49] M. H. Theunissen and P. H. Kes, Resistive transitions of thin film superconductors in a magnetic field, Phys. Rev. B **55**, 15183 (1997).

[50] P. Marra, A. Nigro, Z. Li, G. F. Chen, N. L. Wang, J. L. Luo, and C. Noce, Paraconductivity of the K-doped $SrFe_2As_2$ superconductor, New J. Phys. **14**, 043001 (2012).

[51] R. I. Rey, C. Carballeira, J. Mosqueira, S. Salem-Sugui Jr., A. D. Alvarenga, H.-Q. Luo, X.-Y. Lu, Y.-C. Chen, and F. Vidal, Measurements of the fluctuation-induced in-plane magnetoconductivity at high reduced temperatures and magnetic fields in the iron arsenide $BaFe_{2-x}Ni_xAs_2$, Supercond. Sci. Technol. **26**, 055004 (2013).

[52] D. Sóñora, C. Carballeira, J. J. Ponte, F. Vidal, T. Grenet, and J. Mosqueira, Paraconductivity of granular Al films at high reduced temperatures and magnetic fields, Phys. Rev. B **100**, 104509 (2019).

[53] W. J. Skocpol and M. Tinkham, Fluctuations near superconducting phase transitions, Rep. Prog. Phys. **38**, 1049 (1975).

[54] R. E. Glover, Ideal resistive transition of a superconductor, Phys. Lett. A **25**, 542 (1967).

[55] D. G. Naugle and R. E. Glover, Thickness dependence of the resistive transition of superconducting films, Phys. Lett. A **28**, 611 (1969).

[56] R. E. Glover, Superconducting fluctuation effects above the transition temperature, Physica **55**, 3 (1971).

[57] J. F. Zasadzinski, A. Saggese, K. E. Gray, R. T. Kampwirth, and R. Vaglio, T^4 to T^2 resistivity transition and superconducting fluctuations in disordered VN films, Phys. Rev. B **38**, 5065 (1988).

[58] A. Semenov, B. Günther, U. Böttger, H.-W. Hübers, H. Bartolf, A. Engel, A. Schilling, K. Ilin, M. Siegel, R. Schneider, D. Gerthsen, and N. A. Gippius, Optical and transport properties of ultrathin NbN films and nanostructures, Phys. Rev. B **80**, 054510 (2009).

[59] C. Carbillet, S. Caprara, M. Grilli, C. Brun, T. Cren, F. Debontridder, B. Vignolle, W. Tabis, D. Demaille, L. Largeau, K. Ilin, M. Siegel, D. Roditchev, and B. Leridon, Confinement of superconducting fluctuations due to emergent electronic inhomogeneities, Phys. Rev. B **93**, 144509 (2016).

[60] L. G. Aslamazov and A. I. Larkin, The influence of fluctuation pairing of electrons on the conductivity of normal metal, Phys. Lett. A **26**, 238 (1968).

[61] R. I. Civiak, C. Elbaum, L. F. Nichols, H. I. Kao, and M. M. Labes, Fluctuation-induced conductivity and dimensionality in polysulfur nitride, Phys. Rev. B **14**, 5413 (1976).

[62] J. Kirtley, Y. Imry, and P. K. Hansma, Fluctuation-induced conductivity above the critical temperature in small-particle arrays, J. Low Temp. Phys. **17**, 247 (1974).

[63] K. Maki, Critical fluctuation of the order parameter in a superconductor. I, Prog. Theor. Phys. **40**, 193 (1968).

[64] R. S. Thompson, Microwave, flux flow, and fluctuation resistance of dirty type-II superconductors, Phys. Rev. B **1**, 327 (1970).

[65] W. E. Lawrence and S. Doniach, in *Proceedings of the Twelfth International Conference on Low Temperature Physics*, edited by E. Kanda (Academic Press of Japan, Kyoto, 1971), p. 361.

[66] G. Deutscher, Y. Imry, and L. Gunther, Superconducting phase transitions in granular systems, Phys. Rev. B **10**, 4598 (1974).

[67] S. Wolf and W. H. Lowrey, Zero Dimensionality and Josephson Coupling in Granular Niobium Nitride, Phys. Rev. Lett. **39**, 1038 (1977).

[68] M. Schöck, C. Sürgers, and H. V. Löhneysen, Superconducting and magnetic properties of $Nb/Pd_{1-x}Fe_x/Nb$ triple layers, Eur. Phys. J. B **14**, 1 (2000).

[69] M. Trezza, C. Cirillo, A. L. Dolgiy, S. V. Redko, V. P. Bondarenko, A. V. Andreyenka, A. L. Danilyuk, S. L. Prischepa, and C. Attanasio, Change of the topology of a superconducting thin film electromagnetically coupled with an array of ferromagnetic nanowires, Supercond. Sci. Technol. **29**, 015011 (2016).

[70] J. Guimpel, M. E. de la Cruz, F. de la Cruz, H. J. Fink, O. Laborde, and J. C. Villegier, Size dependence of the superconducting critical temperature and fields of Nb/Al multilayers, J. Low Temp. Phys. **63**, 151 (1986).

[71] S. Lin, O. Ayala-Valenzuela, R. D. McDonald, L. N. Bulaevskii, T. G. Holesinger, F. Ronning, N. R. Weisse-Bernstein, T. L. Williamson, A. H. Mueller, M. A. Hoffbauer, M. W. Rabin, and M. J. Graf, Characterization of the thin-film NbN superconductor for single-photon detection by transport measurements, Phys. Rev. B **87**, 184507 (2013).

[72] X. Zhang, A. Engel, Q. Wang, A. Schilling, A. Semenov, M. Sidorova, H. W. Hubers, I. Charaev, K. Ilin, and M. Siegel, Characteristics of superconducting tungsten silicide W_xSi_{1-x} for single photon detection, Phys. Rev. B **94**, 174509 (2016).

[73] P. H. Kes and C. C. Tsuei, Two-dimensional collective flux pinning, defects, and structural relaxation in amorphous superconducting films, Phys. Rev. B **28**, 5126 (1983).

[74] M. Tinkham, *Introduction to Superconductivity* (McGraw-Hill, Singapore, 1996).

[75] H. Bartolf, A. Engel, A. Schilling, K. Il'in, M. Siegel, H.-W. Hübers, and A. Semenov, Current-assisted thermally activated flux liberation in ultrathin nanopatterned NbN superconducting meander structures, Phys. Rev. B **81**, 024502 (2010).

[76] J. Romijn, T. M. Klapwijk, M. J. Renne, and J. E. Mooij, Critical pair-breaking current in superconducting aluminum strips far below T_c, Phys. Rev. B **26**, 3648 (1982).

[77] M. Y. Kupriyanov and V. F. Lukichev, Temperature dependence of pair-breaking current in superconductors, Sov. J. Low Temp. Phys. **6**, 210 (1980).

[78] D. Dew-Hughes, The critical current of superconductors: an historical review, Low Temp. Phys. **27**, 713 (2001).

[79] J. W. Ekin, Unified scaling law for flux pinning in practical superconductors: I. Separability postulate, raw scaling data and parameterization at moderate strains, Supercond. Sci. Technol. **23**, 083001 (2010).

[80] Md. Matin, L. S. Sharath Chandra, M. K. Chattopadhyay, R. K. Meena, Rakesh Kaul, M. N. Singh, A. K. Sinha, and S. B. Roy, Magnetic irreversibility and pinning force density in the Ti-V alloys, J. Appl. Phys. **113**, 163903 (2013).

[81] E. Martínez, P. Mikheenko, M. Martínez-López, A. Millán, A. Bevan, and J. S. Abell, Flux pinning force in bulk MgB_2 with variable grain size, Phys. Rev. B **75**, 134515 (2007).

[82] R. Wördenweber, Mechanism of fiux-line motion in high-temperature superconductors, Phys. Rev. B **46**, 3076 (1992).

[83] A. I. Larkin and Yu. N. Ovchinnikov, Nonlinear conductivity of superconductors in the mixed state, Sov. Phys. JETP **41**, 960 (1976).

[84] L. Zhang, L. You, W. Penga, Z. Wang, Quasiparticle scattering time in NbN superconducting thin films, Physica C **579**, 1353773 (2020).

[85] C. Attanasio and C. Cirillo, Quasiparticle relaxation mechanisms in superconductor/ferromagnet bilayers, J. Phys.: Condens. Matter **24**, 083201 (2012).

[86] W. Klein, R. P. Huebener, S. Gauss, and J. Parisi, Nonlinearity in the flux-flow behavior of thin-film superconductors, J. Low Temp. Phys. **61**, 413 (1985).

[87] G. Grimaldi, A. Leo, C. Cirillo, A. Casaburi, R. Cristiano, C. Attanasio, A. Nigro, S. Pace, and R. P. Huebener, Nonlinear flux flow resistance of Type-II superconducting films, J. Supercond. Novel Magn. **24**, 81 (2011).

[88] G. Grimaldi, A. Leo, A. Nigro, S. Pace, C. Cirillo, and C. Attanasio, Thickness dependence of vortex critical velocity in wide Nb films, Physica C **468**, 765 (2008).

[89] C. Cirillo, V. Pagliarulo, H. Myoren, C. Bonavolontà, L. Parlato, G. P. Pepe, and C. Attanasio, Quasiparticle energy relaxation times in NbN/CuNi nanostripes from critical velocity measurements, Phys. Rev. B **84**, 054536 (2011).

[90] A. F. Ioffe and A. R. Regel, Non-crystalline, amorphous and liquid electronic semiconductors, Prog. Semicond. **4**, 237 (1960).

[91] Z. Liu and B. Luo, Disorder-induced transport peculiarities in amorphous molybdenum silicide thin films, Phys. Status Solidi B **257**, 2000165 (2020).

[92] J. Chiles, S. M. Buckley, A. Lita, V. Verma, J. Allmaras, B. Korzh, M. D. Shaw, J. M. Shainline, R. P. Mirin, and S. W. Nam, Superconducting microwire detectors based on WSi with single-photon sensitivity in the near-infrared, Appl. Phys. Lett. **116**, 242602 (2020).

[93] A. D. Semenov, G. N. Gol'tsman, and A. A. Korneev, Quantum detection by current carrying superconducting film, Physica C **351**, 349 (2001).

[94] A. Semenov, A. Engel, H.-W. Hübers, K. Il'in, and M. Siegel, Spectral cut-off in the efficiency of the resistive state formation caused by absorption of a single-photon in current-carrying superconducting nano-strips, Eur. Phys. J. B **47**, 495 (2005).

[95] V. B. Verma, B. Korzh, F. Bussieres, R. D. Horansky, A. E. Lita, F. Marsili, M. D. Shaw, H. Zbinden, R. P. Mirin, and S. W. Nam, High-efficiency WSi superconducting nanowire single-photon detectors operating at 2.5 K, Appl. Phys. Lett. **105**, 122601 (2014).

[96] G. G. Taylor, D. Morozov, N. R. Gemmell, K. Erotokritou, S. Miki, H. Terai, and R. H. Hadfield, Photon counting LIDAR at 2.3 μm wavelength with superconducting nanowires, Opt. Express **27**, 38147 (2019).

[97] M. E. Grein, A. J. Kerman, E. A. Dauler, M. M. Willis, B. Romkey, R. J. Molnar, B. S. Robinson, D. V. Murphy, D. M. Boroson, An optical receiver for the Lunar Laser Communication Demonstration based on photon-counting superconducting nanowires, Adv. Photon Counting Techniques IX **9492**, 949208 (2015).

[98] V. B. Verma, B. Korzh, A. B. Walter, A. E. Lita, R. M. Briggs, M. Colangelo, Y. Zhai, E. E. Wollman, A. D. Beyer, J. P. Allmaras, H. Vora, D. Zhu, E. Schmidt, A. G. Kozorezov, K. K. Berggren, R. P. Mirin, S. W. Nam, and M. D. Shaw, Single-photon detection in the mid-infrared up to 10 μm wavelength using tungsten silicide superconducting nanowire detectors, APL Photonics **6**, 056101 (2021).

[99] A. Semenov, A. Engel, K. Il'in, G. Gol'tsman, M. Siegel and H.-W. Hübers, Ultimate performance of a superconducting quantum detector, Eur. Phys. J. Appl. Phys. **21**, 171 (2003).

[100] P. K. Day, H. G. LeDuc, B. A. Mazin, A. Vayonakis, and J. Zmuidzinas, A broadband superconducting detector suitable for use in large arrays, Nature (London) **425**, 817 (2003).

[101] A. V. Moshe, E. Farber, and G. Deutscher, Granular superconductors for high kinetic inductance and low loss quantum devices, Appl. Phys. Lett. **117**, 062601 (2020).